XL CILAMCE
IBERO-LATIN AMERICAN CONGRESS ON COMPUTATIONAL METHODS IN ENGINEERING
NOVEMBER 11-14, 2019
Praiamar Natal Hotel & Convention
Natal, RN-BRAZIL

ATTITUDE CONTROL OF SATELLITE WITH PROPELLANT SLOSHING DYNAMICS

Victoria de Souza Rodrigues
André Fenili
victoria.rodrigues@ufabc.edu.br
andre.fenili@ufabc.edu.br
Centro de Engenharia, Modelagem e Ciências Sociais Aplicadas - UFABC
Av. dos Estados, 5001, 09210-580, Santo André/SP, Brazil

Abstract. Space vehicles can carry large amounts of liquid propellant in their tanks, especially when performing interplanetary missions. When these tanks are not completely filled, the movement of the vehicle excites the propellant such that the free surface of the liquid describes an oscillatory movement. This movement confined inside the tank is known as sloshing. Depending on the type of excitation and the geometry of the tank, the liquid sloshing may have an infinite number of natural frequencies; these frequencies tend, in turn, to excite the movement of the vehicle and, consequently, affect attitude control. This paper investigates the attitude control of a satellite, modeled as a rigid body, whose motion is coupled with the slosh effect of the liquid propellant in its interior, represented by an equivalent mechanical model, in this case a simple pendulum. The equations of motion are obtained through Lagrangian formalism. The excitation frequency is assumed to be remote from resonance. Only small amplitudes of oscillation are allowed for the pendulum, so that the free surface remains planar without rotation of its nodal diameter. Attitude control is investigated for different volumes of liquid in the tank. The control technique used is the Linear Quadratic Regulator (LQR) and the results are obtained numerically.

Keywords: Attitude control, Sloshing, LQR, Equivalent mechanical model

1 Introduction

Many spacecraft require large tanks of liquid propellant for orbit transfers and corrections, and for attitude control, especially when they have a considerable structure or when accomplishing very long missions, such as interplanetary. The fuel of a geostationary satellite, for example, amounts about 40% of its total initial mass in the geostationary transfer orbit [1]. When these propellant tanks are not completely filled, the movement of the vehicle excites the propellant such that the free surface of the liquid describes an oscillatory movement. This movement confined inside the tank is known as sloshing [2]. Depending on the type of excitation and the geometry of the tank, the liquid sloshing may have an infinite number of natural frequencies; these frequencies tend, in turn, to excite the movement of the vehicle and, consequently, affect attitude control and the system stability [3].

Several missions have already failed due to fuel slosh, such as the loss of the ATS-V spacecraft in 1969, the NEAR Shoemaker ignition problem in 2000 [4] and the undamped vibration that caused instability of the SpaceX launch vehicle Falcon-1 in 2007 [5]. The importance of studying spacecraft slosh dynamics is therefore great, and different methodologies propose to investigate how fluid motion and vehicle dynamics can be coupled.

Many studies address sloshing considering all nonlinearities of fluid motion; methods such as Computational Fluid Dynamics and Finite Elements are often used to estimate the coupled slosh-vehicle system responses. But considering the speed and memory limitations of the onboard processors, and the high complexity of spacecraft systems, the study of slosh dynamics can be done from a simpler yet realistic approach known as the equivalent mechanical model, which also allows the investigation of control and the analysis of vehicle stability [3]. Equivalence, in this case, is in the sense of equal resulting forces and moments acting on the liquid propellant tank wall [2].

To model the slosh dynamics of the free surface of a liquid that remains planar without rotation of its nodal diameter during all motion, as shown in item (a) of Fig. (1), one can develop equivalent models represented by a set of simple pendulums or by series of spring-mass dashpot systems. In this case of small fluid oscillations, the satellite excitation frequency is assumed remote from the resonance frequency and the approximation of $sin\theta \approx \theta$ is valid. Nichkawde, Harish and Ananthkrishnan [6] and Reyhanoglu [7], for instance, use the simple pendulum as an equivalent model. For relatively larger oscillations, as shown in item (b) of Fig. (1), motion is described by weakly nonlinear differential equations and the equivalent model adopted is the spherical pendulum, as shown, for example, by Kang and Coverstone [8] and by Yue [9]. Finally, for the modeling of the fluid considering large oscillations and hydrodynamic pressure impacts of the liquid motion close to the free surface, as presented in item (c) of Fig. (1), the spherical pendulum model with impact on the tank wall is adopted and the equations of motion are strongly nonlinear [2].

In order to investigate the attitude control of a spacecraft considering only its planar motion and admitting small oscillations of the system, the coupled vehicle-fluid dynamics is studied in this article from the simple pendulum approach as an equivalent model for the fluid sloshing. In item 2 of this paper, the mathematical modeling of the system is described from Lagrangian formalism. The control chosen for investigation is the Linear-Quadratic Regulator (LQR), presented in more detail in item 3. Items 4 and 5 present the numerical simulations and conclusions, respectively.

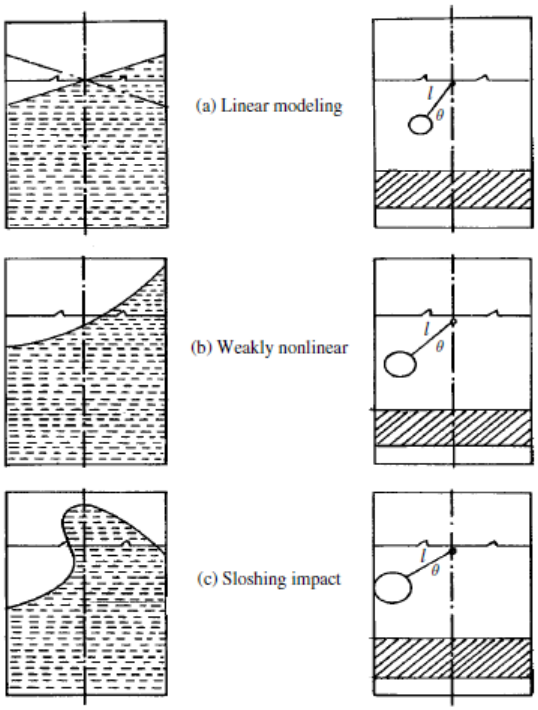

Figure 1. Liquid free surface motion regimes and their equivalent models [2]

2 Mathematical modeling

The model presented here represents the rotational motion of a satellite around the $\vec{Y}$ axis of the adopted inertial coordinate system, described by the angle ψ, as shown in Fig. (2). This angle corresponds to the attitude angle of the satellite, considered here as a rigid body. Inside the vehicle, there is a liquid propellant tank and its fluid is represented by a simple pendulum. The angular displacement of this pendulum from the $\vec{z}$ axis is denoted by θ.

The following model description is based on a similar model presented in [6], which assumes that the vehicle has only planar movements with three degrees of freedom, two translational and one rotational. For slosh modeling, a single vibration mode is considered, so only a single simple pendulum represents the fluid movement. Since the purpose of this paper is attitude control, translational movements are not considered for the system studied, only rotational.

The position vectors of the concentrated masses in the system, as well as their components, are described as:

- $\boldsymbol{r_p}$, illustrated in Fig. (2), is the pendulum mass position vector, m_p, relative to the inertial frame;
- $\boldsymbol{r_{px}}$ is the vector component of $\boldsymbol{r_p}$ in the horizontal direction of the body frame ($\hat{\boldsymbol{i}}$ direction);
- $\boldsymbol{r_{py}}$ is the vector component of $\boldsymbol{r_p}$ in the vertical direction of the body frame ($\hat{\boldsymbol{j}}$ direction);
- $\boldsymbol{r_f}$ is the position vector, described in relation to the inertial frame, of the fluid center of mass moving along with the satellite and not contributing to the slosh effect, also called as "fixed mass", m_f.

The $\boldsymbol{r_p}$ vector components in the body frame can be defined as:

$$\boldsymbol{r_{px}} = Lsin\theta\hat{\boldsymbol{i}}$$

and

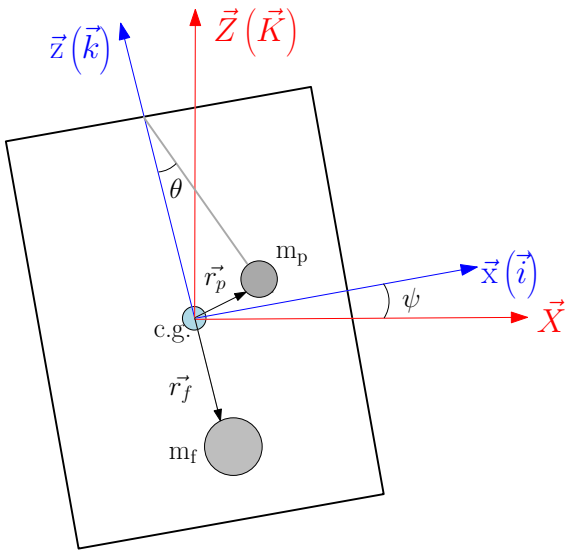

Figure 2. Model of the system studied, indicating the inertial frame in red and the body frame in blue.

$$\boldsymbol{r_{py}} = (b - Lcos\theta)\hat{\boldsymbol{j}},$$

where L is the length of the pendulum mass rod and b is the distance between the pendulum hinge point and the satellite center of gravity, c.g., as shown in (3). So the position vector of the pendulum mass is:

$$\boldsymbol{r_p} = Lsin\theta\hat{\boldsymbol{i}} + (b - Lcos\theta)\hat{\boldsymbol{j}}.$$

The decomposition of the vector $\boldsymbol{r_p}$ in the inertial frame is shown in Eq. (1) and its derivative with respect to time is given in Eq. (2):

$$\boldsymbol{r_p} = [Lsin\theta cos\psi - (b - Lcos\theta)sin\psi]\,\hat{\boldsymbol{I}} + [Lsin\theta sin\psi + (b - Lcos\theta)cos\psi]\,\hat{\boldsymbol{J}}, \tag{1}$$

$$\begin{aligned}\dot{\boldsymbol{r}}_{\boldsymbol{p}} = {} & (Lcos\theta cos\psi\dot{\theta} - Lsin\theta sin\psi\dot{\psi} - bcos\psi\dot{\psi} - Lsin\theta sin\psi\dot{\theta} + Lcos\theta cos\psi\dot{\psi})\hat{\boldsymbol{I}} \\ & + (Lcos\theta sin\psi\dot{\theta} + Lsin\theta cos\psi\dot{\psi} - bsin\psi\dot{\psi} + Lsin\theta cos\psi\dot{\theta} + Lcos\theta sin\psi\dot{\psi})\hat{\boldsymbol{J}}.\end{aligned} \tag{2}$$

The squared norm of $\dot{\boldsymbol{r}}_{\boldsymbol{p}}$ vector is therefore:

$$|\dot{\boldsymbol{r}}_{\boldsymbol{p}}|^2 = L^2\dot{\theta}^2 + L^2\dot{\psi}^2 + b^2\dot{\psi}^2 + 2L^2\dot{\theta}\dot{\psi} - 2bLcos\theta\dot{\theta}\dot{\psi} - 2bLcos\theta\dot{\psi}^2.$$

Similarly, for $\boldsymbol{r_f}$ vector, described in the inertial frame in Eq. (3), the squared norm of its derivative is given by Eq. (4), where h_f is a distance between fixed mass m_f and satellite c.g., as illustrated in Fig. (3).

$$\boldsymbol{r_f} = h_f sin\psi\hat{\boldsymbol{I}} - h_f cos\psi\hat{\boldsymbol{J}} \tag{3}$$

$$|\dot{\boldsymbol{r}}_{\boldsymbol{f}}|^2 = h_f^2 cos^2\psi\dot{\psi}^2 + h_f^2 sin^2\psi\dot{\psi}^2 = h_f^2\dot{\psi}^2 \tag{4}$$

The kinetic energy of the system is composed by the translation of m_p, by the translation and rotational movements of m_f and the rotational motion of the satellite. The fixed mass inertia is I_f and the satellite inertia is I_{sat}, thus:

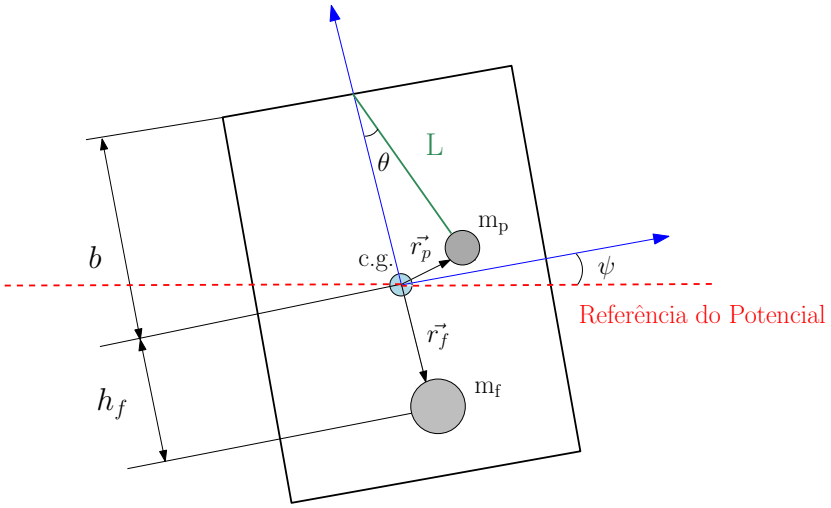

Figure 3. Satellite model studied in this section; highlighted, reference line for the potential energy of the system

$$T = \frac{1}{2}m_p|\dot{\boldsymbol{r}}_{\boldsymbol{p}}|^2 + \frac{1}{2}m_f|\dot{\boldsymbol{r}}_{\boldsymbol{f}}|^2 + \frac{1}{2}I_f\dot{\psi}^2 + \frac{1}{2}I_{sat}\dot{\psi}^2.$$

Potential energy considers the gravitational energies of the pendulum and the fixed mass, as well as the potential deformation energy due to the satellite stiffness for angular (pitch) motion, where k is the stiffness parameter. The gravitational energy of the satellite is not considered because the rotation is around the $\vec{Y}$ axis (perpendicular to the plane of motion), which passes through the satellite center of gravity. Considering g as the acceleration of gravity, the potential energy of the system is given as:

$$V = m_p g\left[Lsen\theta sin\psi + (b - Lcos\theta)cos\psi\right] - m_f g h_f cos\psi + \frac{1}{2}k\psi^2.$$

The Lagrangean $\mathcal{L}$ of the system is given by:

$$\mathcal{L} = T - V,$$

then:

$$\begin{aligned}\mathcal{L} = \frac{1}{2}m_pL^2\dot{\theta}^2 + \frac{1}{2}m_pL^2\dot{\psi}^2 + \frac{1}{2}m_pb^2\dot{\psi}^2 + m_pL^2\dot{\theta}\dot{\psi} - m_pbLcos\theta\dot{\theta}\dot{\psi} \\ - m_pbLcos\theta\dot{\psi}^2 + \frac{1}{2}m_fh_f^2\dot{\psi}^2 + \frac{1}{2}I_f\dot{\psi}^2 + \frac{1}{2}I_{sat}\dot{\psi}^2 - m_pgLsin\theta sin\psi \\ - m_pgbcos\psi + m_pgLcos\theta cos\psi + m_fgh_fcos\psi - \frac{1}{2}k\psi^2.\end{aligned}$$

The system equations of motion are given considering as generalized coordinates the angles ψ and θ. The Euler-Lagrange equations are:

$$\frac{d}{dt}\left(\frac{\partial\mathcal{L}}{\partial\dot{\psi}}\right) - \frac{\partial\mathcal{L}}{\partial\psi} = M_\psi \tag{5}$$

$$\frac{d}{dt}\left(\frac{\partial\mathcal{L}}{\partial\dot{\theta}}\right) - \frac{\partial\mathcal{L}}{\partial\theta} = Q \tag{6}$$

where M_ψ is the satellite pitching moment and Q is the dissipative force of the slosh, given by $Q = -\epsilon\dot{\theta}$, since ϵ is the damping coefficient. Solving Eq. (5), the first system equation of motion, or the satellite equation of motion, is given by:

$$\begin{aligned}\left(m_pL^2 + m_pb^2 - 2m_pbLcos\theta + m_fh_f^2 + I_f + I_{sat}\right)\ddot{\psi} + \left(m_pL^2 - m_pbLcos\theta\right)\ddot{\theta} \\ + \left(2m_pbLsin\theta\dot{\theta}\right)\dot{\psi} + \left(m_pbLsin\theta\dot{\theta}\right)\dot{\theta} + (k)\,\psi + m_pgLsin\theta cos\psi \\ - m_pgbsin\psi + m_pgLcos\theta sin\psi + m_fgh_fsin\psi = M_\psi. \quad (7)\end{aligned}$$

Solving Eq. (6), the second system equation of motion, or the pendulum equation of motion, is given by:

$$\begin{aligned}\left(m_pL^2 - m_pbLcos\theta\right)\ddot{\psi} + \left(m_pL^2\right)\ddot{\theta} + \left(m_pbLsin\theta\dot{\theta} - m_pbLsin\theta\dot{\psi}\right)\dot{\psi} \\ + \left(-m_pbLsin\theta\dot{\psi} + \epsilon\right)\dot{\theta} + m_pgLcos\theta sin\psi + m_pgLsin\theta cos\psi = 0. \quad (8)\end{aligned}$$

Since this model is subject only to small angles ψ, θ, higher order terms can be disregarded, and the following approximations can be made: $cos\psi \approx cos\theta \approx 1$, $sin\psi \approx \psi$ and $sin\theta \approx \theta$. Rewriting Eq. (7):

$$\begin{aligned}\left(m_pL^2 + m_pb^2 - 2m_pbL + m_fh_f^2 + I_f + I_{sat}\right)\ddot{\psi} + \left(m_pL^2 - m_pbL\right)\ddot{\theta} \\ + \left(k - m_pgb + m_pgL + m_fgh_f\right)\psi + \left(m_pgL\right)\theta = M_\psi, \quad (9)\end{aligned}$$

and rewriting Eq. (8):

$$\left(m_pL^2 - m_pbL\right)\ddot{\psi} + \left(m_pL^2\right)\ddot{\theta} + (\epsilon)\,\dot{\theta} + \left(m_pgL\right)\psi + \left(m_pgL\right)\theta = 0. \quad (10)$$

Equation (10) represents the motion of the pendulum mass, so it represents the movement of the fluid portion that contributes to the sloshing in the satellite. Equation (9) represents the satellite movement that can be controlled directly by the torque M_ψ, that is, by the actuators torque. Since the two equations of motion are coupled, the torque M_ψ also acts indirectly on fluid motion. Equations (9) and (10) can be rewritten in matrix form as:

$$\begin{aligned}&\begin{bmatrix} \left(m_pL^2 + m_pb^2 - 2m_pbL + m_fh_f^2 + I_f + I_{sat}\right) & \left(m_pL^2 - m_pbL\right) \\ \left(m_pL^2 - m_pbL\right) & \left(m_pL^2\right) \end{bmatrix}\begin{Bmatrix} \ddot{\psi} \\ \ddot{\theta} \end{Bmatrix} \\ &+ \begin{bmatrix} 0 & 0 \\ 0 & \epsilon \end{bmatrix}\begin{Bmatrix} \dot{\psi} \\ \dot{\theta} \end{Bmatrix} + \begin{bmatrix} \left(k - m_pgb + m_pgL + m_fgh_f\right) & \left(m_pgL\right) \\ \left(m_pgL\right) & \left(m_pgL\right) \end{bmatrix}\begin{Bmatrix} \psi \\ \theta \end{Bmatrix} \\ &= \begin{Bmatrix} M_\psi \\ 0 \end{Bmatrix}. \quad (11)\end{aligned}$$

One can also rewrite Eq. (11) as:

$$\underbrace{\begin{bmatrix} \alpha & \beta \\ \beta & \gamma \end{bmatrix}}_{M}\begin{Bmatrix} \ddot{\psi} \\ \ddot{\theta} \end{Bmatrix} + \begin{bmatrix} 0 & 0 \\ 0 & \epsilon \end{bmatrix}\begin{Bmatrix} \dot{\psi} \\ \dot{\theta} \end{Bmatrix} + \begin{bmatrix} s & uu \\ uu & uu \end{bmatrix}\begin{Bmatrix} \psi \\ \theta \end{Bmatrix} = \begin{Bmatrix} M_\psi \\ 0 \end{Bmatrix}. \quad (12)$$

Inverting the matrix M of Eq. (12), we have:

$$M^{-1} = \begin{bmatrix} \alpha & \beta \\ \beta & \gamma \end{bmatrix}^{-1} = \frac{1}{(-\beta^2 + \alpha\gamma)} \begin{bmatrix} \gamma & -\beta \\ -\beta & \alpha \end{bmatrix}, \tag{13}$$

and multiplying Eq. (12) by Eq. (13), the system equations are described as:

$$\begin{Bmatrix} \ddot{\psi} \\ \ddot{\theta} \end{Bmatrix} + \frac{1}{(-\beta^2 + \alpha\gamma)} \begin{bmatrix} \gamma & -\beta \\ -\beta & \alpha \end{bmatrix} \begin{bmatrix} 0 & 0 \\ 0 & \epsilon \end{bmatrix} \begin{Bmatrix} \dot{\psi} \\ \dot{\theta} \end{Bmatrix} + \frac{1}{(-\beta^2 + \alpha\gamma)} \begin{bmatrix} \gamma & -\beta \\ -\beta & \alpha \end{bmatrix} \begin{bmatrix} s & uu \\ uu & uu \end{bmatrix} \begin{Bmatrix} \psi \\ \theta \end{Bmatrix} = \frac{1}{(-\beta^2 + \alpha\gamma)} \begin{bmatrix} \gamma & -\beta \\ -\beta & \alpha \end{bmatrix} \begin{Bmatrix} M_\psi \\ 0 \end{Bmatrix}. \tag{14}$$

Rewriting the generalized coordinates of Eq. (14) as state space variables:

$$\psi = x_1, \quad \theta = x_3,$$
$$\dot{\psi} = x_2, \quad \dot{\theta} = x_4,$$

and writing Eq. (14) in the form $\dot{x} = Ax + Bu$, the final equations are written as:

$$\begin{Bmatrix} \dot{x}_1 \\ \dot{x}_2 \\ \dot{x}_3 \\ \dot{x}_4 \end{Bmatrix} = \underbrace{\begin{bmatrix} 0 & 1 & 0 & 0 \\ \frac{-\gamma s + \beta uu}{\eta} & 0 & \frac{-\gamma uu + \beta uu}{\eta} & \frac{\beta\epsilon}{\eta} \\ 0 & 0 & 0 & 1 \\ \frac{\beta s - \alpha uu}{\eta} & 0 & \frac{\beta uu - \alpha uu}{\eta} & \frac{-\alpha\epsilon}{\eta} \end{bmatrix}}_{A} \begin{Bmatrix} x_1 \\ x_2 \\ x_3 \\ x_4 \end{Bmatrix} + \underbrace{\begin{bmatrix} 0 \\ \frac{\gamma}{\eta} \\ 0 \\ \frac{-\beta}{\eta} \end{bmatrix}}_{B} M_\psi,$$

where $\eta = -\beta^2 + \alpha\gamma$.

3 Linear-quadratic regulator

The Linear-Quadratic Regulator is an optimal controller designed for systems that have a linear plant in the form given by Eq. (15) and cost function described in the quadratic form, as shown by Eq. (16) [10].

$$\dot{\boldsymbol{x}} = \boldsymbol{A}(t)\boldsymbol{x}(t) + \boldsymbol{B}(t)\boldsymbol{u}(t) \tag{15}$$

$$J = \frac{1}{2} \int_{t_0}^{\infty} \left[\boldsymbol{x}'(t)\boldsymbol{Q}(t)\boldsymbol{x}(t) + \boldsymbol{u}'(t)\boldsymbol{R}(t)\boldsymbol{u}(t) \right] dt \tag{16}$$

Matrix $\boldsymbol{A}(t)$ is the matrix of states and order nxn, matrix $\boldsymbol{B}(t)$ is the matrix of control and order nxr, matrix $\boldsymbol{Q}(t)$ is the matrix that weighs the system error and must always be positive semi-definite and $\boldsymbol{R}(t)$ matrix is the control-weighting matrix and must always be positive definite.

Since the control vector $\boldsymbol{u}(t)$ is not constrained, the end state vector being given as $\boldsymbol{x}(t_f)$ and the end time t_f, the optimal control is given as:

$$\boldsymbol{u}^*(t) = -\boldsymbol{R}^{-1}(t)\boldsymbol{B}(t)\boldsymbol{P}(t)\boldsymbol{x}^*(t), \tag{17}$$

where $\boldsymbol{P}(t)$ is the differential solution of the Riccati equation, which is:

$$\boldsymbol{P}(t) = -\boldsymbol{P}(t)\boldsymbol{A}(t) - \boldsymbol{A'}(t)\boldsymbol{P}(t) - \boldsymbol{Q}(t) + \boldsymbol{P}(t)\boldsymbol{B}(t)\boldsymbol{R}^{-1}(t)\boldsymbol{B'}(t)\boldsymbol{P}(t), \tag{18}$$

satisfying the final condition:

$$\boldsymbol{P}(t = t_f \to \infty) = 0. \tag{19}$$

The optimal state vector is the solution of Eq. (20) and the optimal perfomance index is given by Eq. (21).

$$\dot{\boldsymbol{x}}^*(t) = \left[\boldsymbol{A}(t) - \boldsymbol{B}(t)\boldsymbol{R}^{-1}(t)\boldsymbol{B'}(t)\boldsymbol{P}(t)\right]\boldsymbol{x}^*(t) \tag{20}$$

$$J^* = \frac{1}{2}\boldsymbol{x}^{*'}(t)\boldsymbol{P}(t)\boldsymbol{x}^*(t) \tag{21}$$

Since the time interval considered in Eq. (16) is infinite, the system given by Eq. (15) must be completely controllable for optimal control to be found.

4 Numerical simulations

The simulations presented in this section were done using MATLAB (MATrix LABoratory) software with the fourth order Runge-Kutta method for numerical integration. The iteration step used in all simulations is $h = 0.001$. The system parameter values considered in the numerical simulations are presented in Table (1). The acceleration of gravity is calculated for the altitude of 400 km above sea level.

Table 1. Parameter values used in numerical simulations

Case	m_p (kg)	m_f (kg)	L (m)	b (m)	h_f (m)	I_f (kg.m²)
1	180	150	0.33	-0.50	0.50	0
2	180	650	0.27	0	0.30	30
3	180	850	0.27	0.25	0.20	60

The objective of these simulations is to present three different system configurations and to show, first, a comparison between the natural response of the system against the controlled response for each case; then, a comparison of the control effort between them. The parameters presented in Table (1) were taken based on the graphs presented by Li, Ma and Wang [11].

Case 1 is characterized by the configuration where the pendulum hinge point is below the satellite center of gravity, i.e., $b < 0$. Case 2 has the pendulum hinge point at the same point as the satellite c.g. ($b = 0$) and Case 3 has the pendulum hinge point above c.g. ($b > 0$).

For the three cases, the initial conditions of the state variables are:

$$x_1 = 0.57°, x_2 = 0°/s, x_3 = 1°, x_4 = 0°/s$$

and the control matrices Q and R are given as:

$$Q = \begin{bmatrix} 100 & 0 & 0 & 0 \\ 0 & 100 & 0 & 0 \\ 0 & 0 & 100 & 0 \\ 0 & 0 & 0 & 100 \end{bmatrix}, R = 0.01.$$

Figures (4) and (5) present the angular responses of Case 1. In them, it is possible to observe that the natural response of the system is very oscillatory, and the pendulum responses, specifically, show that the system loses energy over time, but does not accommodate before 100 seconds. With the LQR control, both satellite and pendulum converge to the origin in approximately 60 seconds.

The answers from Case 3, presented in Fig. (8) and Fig. (9), are similar to Case 1: naturally the system has an oscillatory behavior that appears to slowly lose energy and, with the action of the LQR control, the system reaches steady state before 100 seconds.

The answer of Case 2, in turn, presents a natural behavior similar to the previous ones (as shown in Fig. (6) and Fig. (7)), but when under the LQR control, it differs considerably; the response of the satellite position and velocity indicates that the attitude has converged to the reference, but the pendulum still oscillates much like the behavior without control.

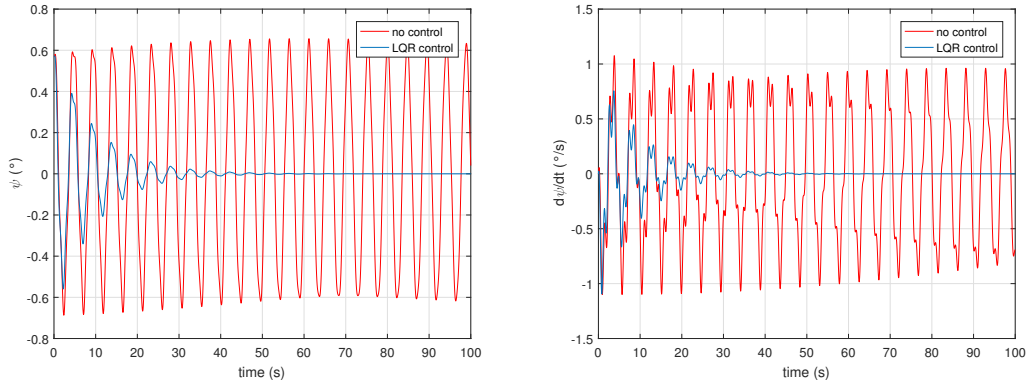

(a) (b)

Figure 4. System dynamics without and with LQR control for Case 1, where (a) is the pitch angle response ψ and (b) is the pitch angle velocity response $\dot{\psi}$

Figure (10) presents the control effort response of each of the three cases. In the graph, it is possible to notice that the responses of cases 1 and 3 are similar: both are quite oscillatory in the transient regime, but reach steady state in approximately 50 seconds for Case 1 and 70 seconds for Case 3. Regarding the amplitude of the oscillation , Case 3 is slightly larger than Case 1. For Case 2, the answer has another feature: low oscillation in the first 40 seconds of simulation and about 5 times smaller than in previous cases, but still appearing to oscillate very small, virtually negligible up to 200 seconds.

5 Conclusions

A satellite model considering the fluid sloshing dynamics was proposed using a simple pendulum to represent the oscillatory motion of the liquid propellant. The behavior of its natural dynamics was analyzed for three different pendulum position settings in relation to the satellite center of gravity in the model. This natural behavior, in all three cases, was oscillatory with

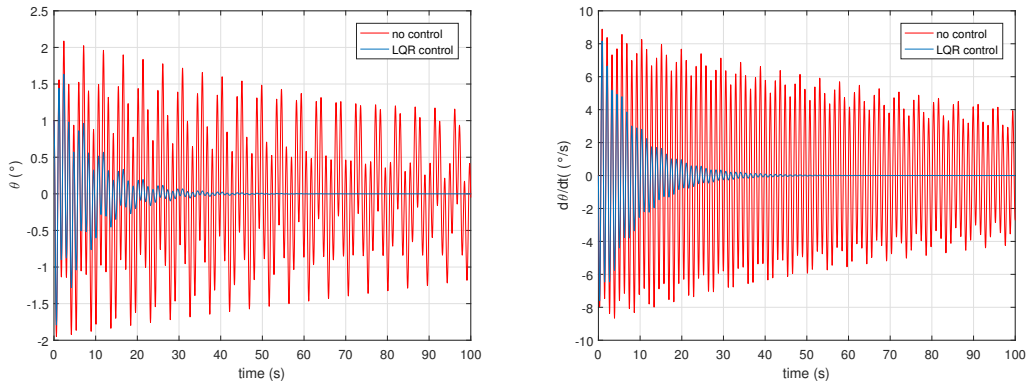

(a) (b)

Figure 5. System dynamics without and with LQR control for Case 1, where (a) is the pendulum angle response and (b) is the pendulum angular velocity response

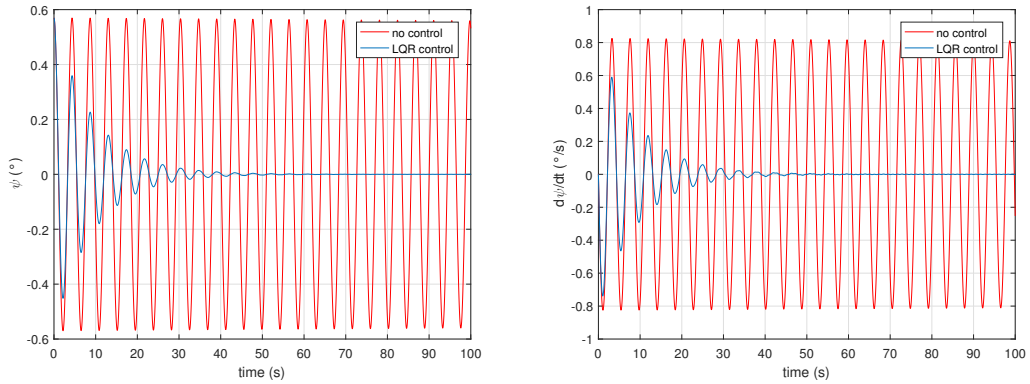

(a) (b)

Figure 6. System dynamics without and with LQR control for Case 2, where (a) is the pitch angle response ψ and (b) is the pitch angle velocity response $\dot{\psi}$

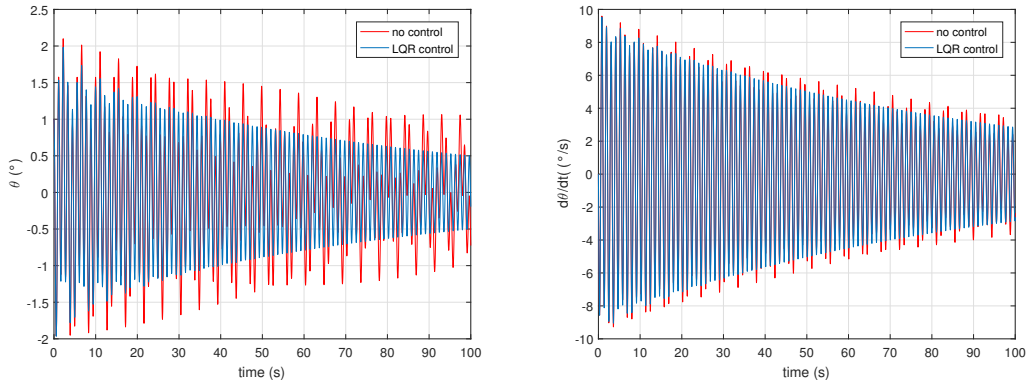

(a) (b)

Figura 7. System dynamics without and with LQR control for Case 2, where (a) is the pendulum angle response and (b) is the pendulum angular velocity response

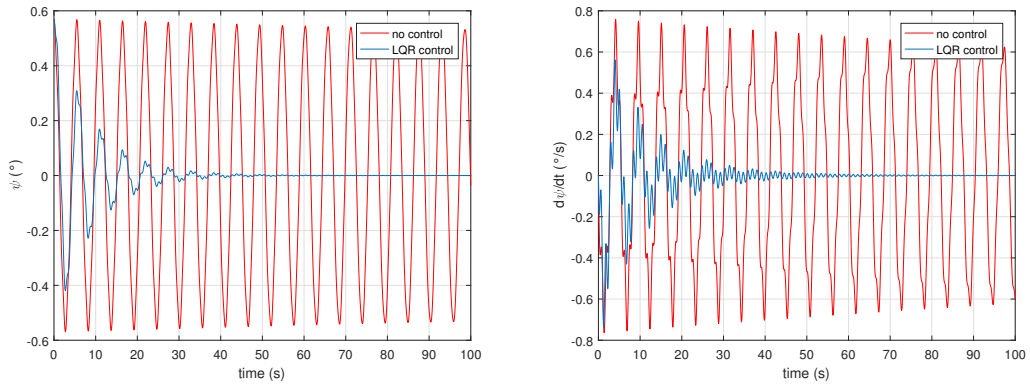

(a) (b)

Figura 8. System dynamics without and with LQR control for Case 3, where (a) is the pitch angle response ψ and (b) is the pitch angle velocity response $\dot{\psi}$

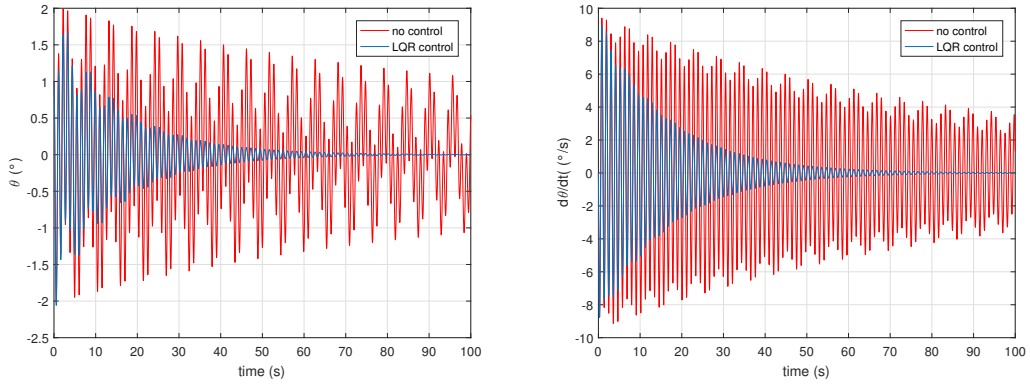

(a) (b)

Figure 9. System dynamics without and with LQR control for Case 3, where (a) is the pendulum angle response and (b) is the pendulum angular velocity response

energy loss for all state variables. With the action of the LQR control, cases 1 and 3 were similar, showing that the control not only led to the attitude for its reference, but also stabilized the movement of the fluid (pendulum). For Case 2, the attitude was also stabilized, but for the given simulation time, the pendulum still had an oscillation similar to the natural dynamics of the system, still far from reaching steady state. Analyzing the torques involved in the problem, it can be seen that, for both cases 1 and 3, the position of the pendulum hinge point is not coincident with the center of gravity and therefore allows a torque beyond that already found in the system due to the fixed mass m_f (which in all cases is below the c.g.). For Case 2, since there is no distance between b and c.g., the decomposition of the pendulum mass position vector falls on the satellite's symmetry axes, thus allowing no torque other than that produced by the mass m_f. On the other hand, precisely because of the absence of the pendulum torque, the control effort required to bring the attitude to the desired position is about 5 times lower for Case 2 than the others.

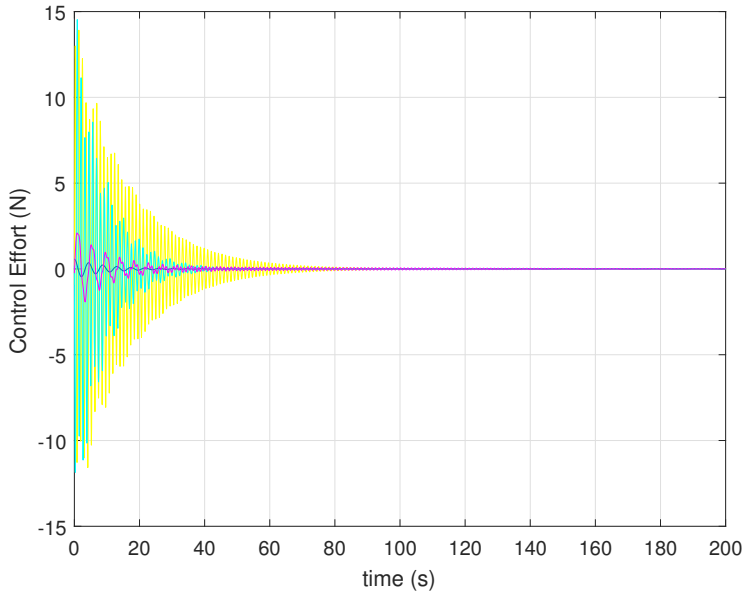

Figure 10. Control effort comparison between the three different cases

Acknowledgements

This research was supported by Coordenação de Aperfeiçoamento de Pessoal de Nível Superior (CAPES).

References

[1] Sidi, M. J., 1997. *Spacecraft Dynamics and Control: A Practical Engineering Approach (Cambridge Aerospace Series)*. Cambridge University Press. 1

[2] Ibrahim, R. A., 2005. *Liquid Sloshing Dynamics*. Cambridge University Press. 1, 1

[3] Cui, D.-L., Yan, S.-Z., Guo, X.-S., & Gao, R. X., 2014. Parametric resonance of liquid sloshing in partially filled spacecraft tanks during the powered-flight phase of rocket. *Aerospace Science and Technology*, vol. 35, pp. 93–105. 1

[4] Shageer, H. & Tao, G., 2007. Modeling and adaptive control of spacecraft with fuel slosh: Overview and case studies. In *AIAA Guidance, Navigation and Control Conference and Exhibit*. American Institute of Aeronautics and Astronautics. 1

[5] Sances, D., Gangadharan, S., Sudermann, J., & Marsell, B., 2010. CFD fuel slosh modeling of fluid-structure interaction in spacecraft propellant tanks with diaphragms. In *51st AIAA/ASME/ASCE/AHS/ASC Structures, Structural Dynamics, and Materials Conference&ltBR&gt 18th AIAA/ASME/AHS Adaptive Structures Conference&ltBR&gt 12th*. American Institute of Aeronautics and Astronautics. 1

[6] Nichkawde, C., Harish, P., & Ananthkrishnan, N., 2004. Stability analysis of a multibody system model for coupled slosh–vehicle dynamics. *Journal of Sound and Vibration*, vol. 275, n. 3-5, pp. 1069–1083. 1, 2

[7] Reyhanoglu, M., 2011. Modelling and control of space vehicles with fuel slosh dynamics. In *Advances in Spacecraft Technologies*. InTech. 1

[8] Kang, J.-Y. & Coverstone, V. L., 2010. Analytical model for momentum transfer of spacecraft containing liquid. *Journal of Guidance, Control, and Dynamics*, vol. 33, n. 3, pp. 991–994. 1

[9] Yue, B.-Z., 2011. Study on the chaotic dynamics in attitude maneuver of liquid-filled flexible spacecraft. *AIAA Journal*, vol. 49, n. 10, pp. 2090–2099. 1

[10] Naidu, D. S., 2002. *Optimal Control Systems*. CRC Press. 3

[11] Li, Q., Ma, X., & Wang, T., 2011. Equivalent mechanical model for liquid sloshing during draining. *Acta Astronautica*, vol. 68, n. 1-2, pp. 91–100. 4